INORGANIC CHEMISTRY FRONTIERS

RESEARCH ARTICLE

View Article Online
View Journal | View Issue

Cite this: *Inorg. Chem. Front.*, 2024, **11**, 5709

Supracluster assembly of an Al_4 precursor toward the study of enhanced optical properties†

Fan Yang,‡[a,b] Rui-Yan Chen,‡[a,c] San-Tai Wang,[a,b] Yan-Ping He, *[a] Wei-Hui Fang *[a,b] and Jian Zhang [a]

Received 5th May 2024,
Accepted 17th July 2024

DOI: 10.1039/d4qi01103a

rsc.li/frontiers-inorganic

Supracluster assembly offers a unique opportunity for the isolation of customized materials using functional cluster precursors. Herein, for the first time, we demonstrate supracluster assembly based on an Al_4^{4-} precursor through both non-covalent interactions and coordination bonds. By reacting readily available, ultrastable, and soluble Al_4^{4-} as an anionic precursor with a metal center and neutral chelated chromophores, we successfully synthesized an extensive library of supracluster assembled crystalline solids, ranging from ion-pair structures, surface-modified clusters, and chains, to layered compounds. The advantage of this method is that it achieves stepwise performance regulation and enhancement using given functional precursors. These materials from supracluster assembly possess a broad range of tunable photophysical properties, including photoluminescence and third-order nonlinear optical (NLO) properties. Such extraordinary supracluster assembly will be widely applicable for creating a new generation of rationally organized solid materials with tailorable and customized properties.

Introduction

Post-synthetic modification is a useful technique to precisely prepare new target materials by introducing desired properties into pre-designed structures.[1–3] Such a method involves introducing small organic molecules or polymers, metal ions, *etc.* into pre-synthesized materials without destroying the structure of the material itself so as to obtain new functional materials. Therefore, it is prevalent and widely used in a broad range of materials, including metal–and covalent organic frameworks,[1,3–5] porous- and metal–organic cages,[2,6] and interlocked molecules.[7]

The molecular nature of discrete metal–organic cages and cluster compounds endows them with easy solution-processability unattainable with traditional framework materials.[8] Thus, these discrete compounds can be adapted for stepwise assembly through solution processing in addition to the solid state. In this regard, the stepwise approach involves dissolving these discrete supramolecular entities in an appropriate solvent and then reacting them with the desired functional element in covalent, coordinated and noncovalent ways.[6] Typical representatives are tetrahedral Ti-,[9–13] Zr-,[8,14–19] Fe-,[20–22] and Ln-based cages,[23,24] cuboctahedral Cr-based cages, *etc.*[25–27] The most distinguished representative in cluster science is polyoxometalates.[28–33] However, the stepwise assembly method based on main group metal clusters has not been effectively developed. Typical examples include the assembly of anionic $[V_{10}O_{28}]^{6-}$/$[\alpha\text{-}1,2,3\text{-}\alpha\text{-}1,2,3\text{-}SiV^V_3W_9O_{40}]^{7-}$ and cationic $[AlO_4Al_{12}(OH)_{24}(H_2O)_{12}]^{7+}$ clusters.[34,35]

Recently, we reported the supracluster assembly of Archimedean $\{Al_6M_3\}_8$ cages with 72 hydrogen bonds.[36] The supracluster assembly fills the gap between "supramolecular"[37] and "superparticle"[38] systems. The word "supracluster" is rarely used but was once used to describe and emphasize the size of clusters, where Teo and Dale named compounds $[(Ph_3P)_{10}Au_{12}Ag_{12}PtCl_7]Cl$ and $[Ru_6C(CO)_{17}]$ in 1993 and 1995,[39,40] whereas our proposed supracluster assembly aims to achieve "chemistry beyond the cluster", in that attention should be paid to the interactions between clusters, such as hydrogen bonds, π···π interactions and covalent bonds, with the interactions between the vertex and edge-sharing supracluster assemblies based on Archimedean $\{Al_6M_3\}_8$ cages being hydrogen bonds. In our previous work, we investigated the coordination-driven self-assembly of aluminum molecular rings, which can be viewed as supracluster assembly *via* coordination bonds.

Herein, for the first time, we demonstrate supracluster assembly based on an Al_4 precursor through both hydrogen

[a]*State Key Laboratory of Structural Chemistry, Fujian Institute of Research on the Structure of Matter, Chinese Academy of Sciences, 350002 Fuzhou, P.R. China. E-mail: hyp041@163.com, fwh@fjirsm.ac.cn*
[b]*University of Chinese Academy of Sciences, Beijing 100049, China*
[c]*MOE Key Laboratory of Cluster Science, School of Chemistry and Chemical Engineering, Beijing Institute of Technology, Beijing 100081, China*
† Electronic supplementary information (ESI) available. CCDC 2303391–2303400. For ESI and crystallographic data in CIF or other electronic format see DOI: https://doi.org/10.1039/d4qi01103a
‡ These authors contributed equally to this work.

bonds and coordination bonds. Based on our recent efforts and progress in aluminum oxo clusters (AlOCs),[41–47] we believe that $(Me_2NH_2)_4[Al_4(L)_4(Cat)_2]$ (**AlOC-13**, a cluster denoted as Al_4 hereinafter)[42] is a suitable precursor for further study of supracluster assembly of target materials with photo-related properties (Scheme 1) where (1) it fulfills the requirements of high solubility/stability and accessibility for scale-up synthesis; and (2) it provides one successful example of incorporating lanthanides[42] proving the possibility of assembly and that the abundance of interaction sites (aromatic ring, hydroxyl group and bridging oxo) will bring more interesting modes of assembly. The presence of aromatic rings and an oxo moiety may lead to weak interaction with guest molecules. The suspended oxo group may result in coordination with oxyphilic metal ions. Such assembly is feasible from the point of view of charge matching. We selected a series of chelating ligands of different lengths, and the distance between the two chelating sites plays a key role in assembling the compound type to form ion pairs and coordination-modified compounds, respectively. With subsequent assembly, the photo-related properties will also be tuned. Accordingly, we probe an avenue toward the enhancement of intended optical properties like photoluminescence and third-order nonlinear optical (NLO) effects. For example, the employment of chiral ligands and heavy metal ions enhances third-order NLO performance.[48,49]

Results and discussion

Synthesis

The facile synthesis of large amounts of **AlOC-13** as the source of the Al_4 clusters is described in detail in the Experimental section (Scheme S1 and Tables S1–S3†). It is a monodisperse anionic cluster with $(Me_2NH_2)^+$ countercations, which can be soluble and stable in water and common solvents. There are eight uncoordinated carboxyl oxygen atoms and six phenyl rings in each Al_4 cluster, making it an excellent precursor for assembly with cationic units. The reasons we chose the N,N-chelated (phenanthroline-type) and P,P-chelated (phenylphosphine-type) ligands are that they meet the requirements of both ligand chelate and photo-functional conjugated groups (Fig. 1). By investigating the supracluster assembly behaviors of Al_4 clusters with metal ions (such as Ag^+, Fe^{2+} and Cu^{2+}), we successfully obtained a variety of novel ionic pair compounds *via* short chelating ligands (hydrogen bonds and π···π interactions) (**AlOC-168** to **AlOC-172**) and coordination-modified compounds through relatively long chelating ligands (**AlOC-173** to **AlOC-176**) (Table 1). Rapid crystal growth of these materials can be achieved by solvent-thermal synthesis in one day.

Supracluster assembly of structures *via* non-covalent bonds

In the beginning, $AgClO_4$ and the 1,3-bdpp ligand were added to a DMF/EtOH/H_2O solution of the Al_4 precursor, which was kept at 80 °C for one day, yielding faint yellow block crystals of **AlOC-168.** In the structure of **AlOC-168**, the Ag(I) center is P,P-chelated by two 1,3-bdpp ligands, giving rise to an $[Ag(1,3\text{-bdpp})_2]^+$ ion (Fig. S1†). The supracluster assembly of the

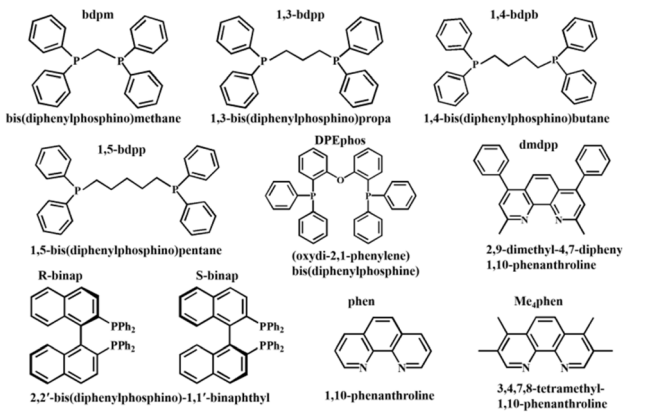

Fig. 1 The N,N-chelated or P,P-chelated ligands used in the supramolecular assembly based on Al_4 clusters.

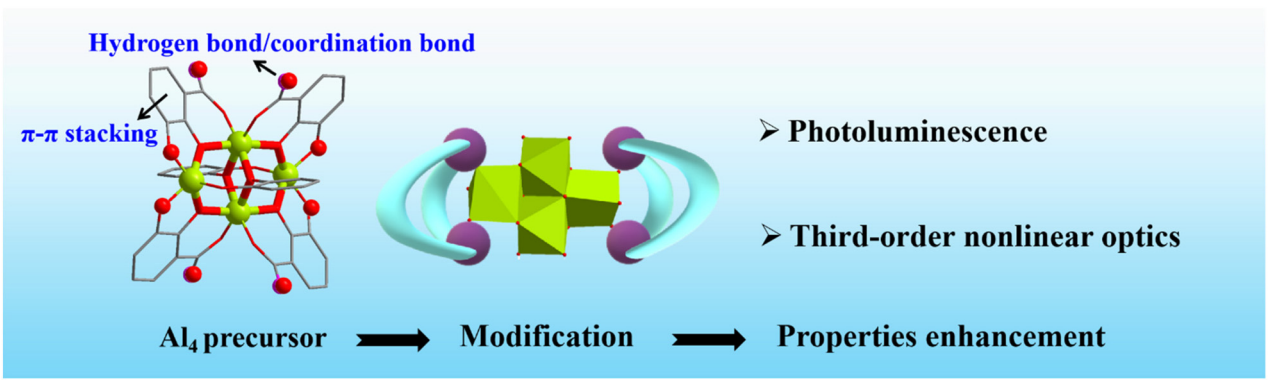

Scheme 1 Illustration of the selection of the Al_4 precursor and its supracluster assembly towards enhancement of photo-related properties. The advantages of using the Al_4 precursor include its high solubility/stability and accessibility for scale-up synthesis, as well as abundant binding sites. The supracluster assembly method includes non-covalent interaction assembly and coordination bond interaction assembly. The dark purple balls represent metal centers like Ag^+, Fe^{2+} and Cu^{2+}, while the cyan loops represent flexible ligands.

Table 1 Summary of the compounds resulting from the supracluster assembly of the Al_4 precursor

Complex	Composition	Space group	Structure dimensionality	R_1 value	CCDC
Supracluster assembly of structures *via* non-covalent bonds					
AlOC-168	$(Me_2NH_2)_3[Ag(1,3\text{-bdpp})_2][Al_4(L)_4(Cat)_2]$	$P\bar{1}$	0D	0.053	2303391
AlOC-169	$(Me_2NH_2)_3[Ag(dmdpp)(DPEphos)][Al_4(L)_4(Cat)_2]$	*Pbca*	0D	0.138	2303392
AlOC-170(R)	$(Me_2NH_2)_6[Ag(R\text{-binap})_2]_2[Al_4(L)_4(Cat)_2]_2$	$P2_1$	0D	0.077	2303393
AlOC-170(S)	$(Me_2NH_2)_6[Ag(S\text{-binap})_2]_2[Al_4(L)_4(Cat)_2]_2$	$P2_1$	0D	0.053	2303394
AlOC-171	$[Fe(phen)_3]_2[Al_4(L)_4(Cat)_2]$	*I*2/*a*	0D	0.041	2303395
AlOC-172	$[Cu(Me_4phen)_2(H_2O)]_2[Al_4(L)_4(Cat)_2]$	$P\bar{1}$	0D	0.051	2303396
Supracluster assembly of structures *via* coordination bonds					
AlOC-173	$[Ag_2(bdpm)_2]_2[Al_4(L)_4(Cat)_2]$	$P\bar{1}$	0D	0.053	2303397
AlOC-174	$[Ag_3(1,5\text{-bdpp})_3]_2[Al_4(L)_4(Cat)_2](ClO_4)_2$	$P\bar{1}$	0D	0.043	2303398
AlOC-175	$[Ag_4(1,4\text{-bdpb})_3][Al_4(L)_4(Cat)_2]$	*I*2/*a*	1D	0.036	2303399
AlOC-176	$[Ag_4(bdpm)_2(1,4\text{-bdpb})][Al_4(L)_4(Cat)_2]$	$P\bar{1}$	2D	0.042	2303400

H_3L = 2,3-dihydroxybenzoic acid; cat = catechol; bdpm = bis(diphenylphosphino)methane; 1,3-bdpp = 1,3-bis(diphenylphosphino)propane; 1,4-bdpb = 1,4-bis(diphenylphosphino)butane; 1,5-bdpp = 1,5-bis(diphenylphosphino)pentane; DPEphos = (oxydi-2,1-phenylene)bis(diphenylphosphine); *R*-binap = (*R*)-(+)-2,2′-bis(diphenylphosphino)-1,1′-binaphthyl; *S*-binap = (*S*)-(−)-2,2′-bis(diphenylphosphino)-1,1′-binaphthyl; phen = 1,10-phenanthroline; dmdpp = 2,9-dimethyl-4,7-diphenyl-1,10-phenanthroline; Me4phen = 3,4,7,8-tetramethyl-1,10-phenanthroline.

anionic Al_4 cluster and cationic $[Ag(1,3\text{-bdpp})_2]^+$ unit forms an interesting ion-pair structure (Fig. 2a). However, in the above synthetic system of **AlOC-168**, we replaced the 1,3-bdpp ligand with DPEphos and added the dmdpp phenanthroline-type ligand, and we readily obtained another ion-pair structure (**AlOC-169**) composed of an Al_4 cluster and $[Ag(dmdpp)(DPEphos)]^+$ unit (Fig. S4†), in which the Ag(I) center is chelated by one DPEphos ligand and one dmdpp ligand. When we replaced the organic ligand with a chiral binap ligand, we successfully synthesized a pair of pure enantiomers (**AlOC-170(*R*)**

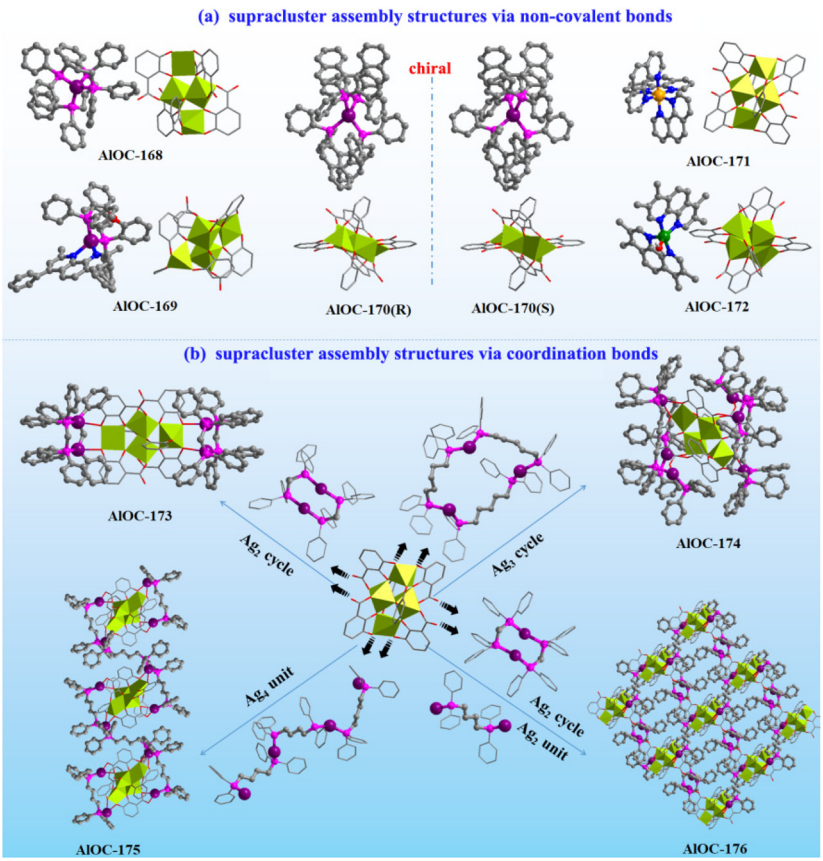

Fig. 2 A family of structures from supracluster assembly based on pre-designed Al_4 clusters including (a) supracluster assembly of structures *via* non-covalent bonds and (b) supracluster assembly of structures *via* coordination bonds. Atom color code: green, Al; modena, Ag; orange, Fe; olive, Cu; pink, P; red, O; blue, N; gray, C; off-white, H.

and **AlOC-170(*S*)**) (Fig. S7 and S10†). In their structures, two *R*- or *S*-binap ligands coordinate to one Ag(I) center, producing a chiral $[Ag(R\text{-binap})_2]^+$ or $[Ag(S\text{-binap})_2]^+$ unit, which further forms chiral ion-pair structures with the Al_4 cluster. Their absolute configuration and enantiomeric nature have been confirmed by circular dichroism (CD) spectra, whose CD peaks exhibit obvious mirror images (Fig. S61†). Considering the chiral and fluorescent properties of **AlOC-170*R*/*S***,[50,51] we tested their circularly polarized luminescence, and the results were not as expected. In the 3D packing structures of **AlOC-168** to **AlOC-170**, there are multiple supramolecular interactions, including π···π stacking and C–H···π, C–H···O, O–H···O, and N–H···O interactions (Fig. S3, S6 and S9†). It is particularly necessary to point out that the Ag units form a cationic layer, while the Al_4 clusters form an anionic layer (Fig. S2, S5 and S8†), and they take the ABAB alternating stacking mode, which is similar to that of hydrotalcite. Furthermore, the $(Me_2NH_2)^+$ countercations are located in the anionic Al_4 cluster layer. By replacing the above $AgClO_4$ with $FeSO_4{\cdot}7H_2O$ and Cu_2O and adding a small amount of ammonium hydroxide, we synthesized ion-pair structures **AlOC-171** and **AlOC-172** in the presence of phen and Me_4phen ligands, respectively. The Fe(II) and Cu(II) centers are N,N-chelated by two phen and Me_4phen ligands (Fig. S11 and S13†), respectively, and there is also an H_2O molecule that coordinates to the Cu(II) center. Through weak interactions, the Al_4 clusters and the $[Fe(phen)_3]^{2+}$ or $[Cu(Me_4phen)_2(H_2O)]^{2+}$ cations stack alternately into a 3D dense structure (Fig. S12 and S14†).

Supracluster assembly of structures *via* coordination bonds

Encouraged by the above results, more assembly experiments were explored (Fig. 2b). When increasing the dosage of Ag^+ ions and using the shorter bdpm ligand, we synthesized **AlOC-173**. In the structure of **AlOC-173** (Fig. S15 and S16†), two Ag(I) centers are connected by two bdpm ligands, *in situ* forming a binuclear $[Ag_2(bdpm)_2]^{2+}$ cycle (named the Ag_2 cycle). Interestingly, each Al_4 cluster links two such Ag_2 cycles *via* the Ag–O coordination bond on both sides of the cluster, in which the carboxyl O atoms of the Al_4 cluster coordinate to the Ag(I) atom of the Ag_2 cycle. The Ag···Ag length is about 2.9 Å, and the Ag–O bond lengths are about 2.5 Å, which are within the normal bond-length range. All the Ag(I) centers are three-coordinated. As we continued to increase the dosage of Ag^+ ions and used a longer 1,5-bdpp ligand, we obtained **AlOC-174**. Structural analyses show that each Al_4 cluster in **AlOC-174** traps two *in situ* formed $[Ag_3(1,5\text{-bdpp})_3]^{3+}$ cycles (each named as an Ag_3 cycle). As shown in Fig. S17,† the Ag1 atom is four-coordinated, while Ag2 and Ag3 atoms are three-coordinated. The $(ClO_4)^-$ counteranions are present in the structure of **AlOC-174** (Fig. S18†). Herein, through coordination interactions, we modified the Ag_2 and Ag_3 cycles onto the Al_4 cluster and obtained two functional ligand-modified heterometallic clusters.

From the above results, it can be seen that the length of the organic ligand also affected the supracluster assembly behavior of the Al_4 cluster, so we continued to change the type of ligand and tried using mixed organic ligands. When the 1,4-bdpb ligand was used to react with Ag^+ ions and Al_4 clusters, **AlOC-175** was synthesized. In **AlOC-175**, three 1,4-bdpb ligands link with four Ag(I) centers to generate a tetranuclear $[Ag_4(1,4\text{-bdpb})_3]^{4+}$ unit (named the Ag_4 unit) (Fig. S19†). Such an *in situ* generated Ag_4 unit further connects two adjacent Al_4 clusters through Ag–O coordination bonds, giving rise to an infinite chain structure. The chains are stacked in ABAB mode to form a dense supramolecular structure (Fig. S20†), and there are rich interactions between adjacent chains in **AlOC-175**, including π···π stacking, C–H···π and C–H···O interactions. However, when longer 1,4-bdpb and shorter bdpm ligands were added to the reaction system simultaneously, we obtained compound **AlOC-176**. Structural analysis shows that **AlOC-176** has a layered structure of Al_4 clusters linked together by $[Ag_2(bdpm)_2]^{2+}$ cycles (named the Ag_2 cycle) and $[Ag_2(1,4\text{-bdpb})]^{2+}$ units (named the Ag_2 unit) (Fig. S21†). In the structure of **AlOC-173**, the Ag_2 cycle is only modified at both ends of the cluster, while it acts as a linker in **AlOC-176**, collaborating with the Ag_2 unit to further connect with and form the Al_4 clusters into a layer (Fig. S22†).

Herein, we demonstrated an extraordinary supracluster assembly including both non-covalent and coordination bonds. These assembled compounds are challenging to synthesize in one pot, so through supracluster assembly, we can indeed obtain new materials that cannot be obtained by direct synthesis. In theory, all kinds of metal cation units can form ion-pair structures with the anionic Al_4 cluster. Similarly, coordination bonds can also modify different metal cation units at the face of the cluster. On the other hand, the Al_4 cluster can also be organized into different dimensional structures, including chain and layer structures, as well as 3D frameworks. Through functional modification, we can obtain the desired applications.

The powder X-ray diffraction (XRD) patterns of **AlOC-168** to **AlOC-176** are shown in Fig. S23–S31.† To ensure the high purity of all structures, we performed Le Bail fitting. The low R_{wp} and R_p values (<10%) in the Le Bail fittings show that these compounds have high phase purity, indicating that the self-assembly of Al_4 clusters with metal cation units into these cluster-based compounds under certain conditions is quite stable and directed. The thermogravimetric analysis (TGA) curves of these materials were recorded, as shown in Fig. S32–S40 in the ESI.† Their TG curves do not have a relatively apparent weightless platform before 300 °C, which is consistent with their dense supramolecular packing structures. The solvents or counterions ($(Me_2NH_2)^+$ or $(ClO_4)^-$) were gradually lost with increasing temperature, followed by decomposition of their structures. The residues after decomposition might be Ag_2O and CuO or Fe_3O_4. Diffuse reflectance spectroscopy was used to study the UV/vis absorption of these compounds. According to the Kubelka–Munk function, yellowish Ag-cluster- and green Cu-cluster-based compounds exhibit relatively low bandgaps (2.6–3.1 eV) compared to that of the Al_4 cluster raw material (3.2 eV), but that of the deep red **AlOC-171**, containing the $[Fe(phen)_3]^{2+}$ unit, is about 1.56 eV,

which is significantly lower than that of other compounds (Fig. 3a, b and S42–S50†). Their homogeneous elemental distribution was confirmed by their spectra from energy dispersive spectroscopy (EDS) as shown in Fig. S51–S58.†

Studies of photoluminescence properties

Because the phenanthroline- and phenylphosphine-type ligands possess strong absorbing chromophores, and the Ag-based compounds themselves have good photoluminescent properties, we decided to study the solid-state excitation and emission spectra of compounds **AlOC-168** to **AlOC-176** at room temperature (Fig. 3c and d). For convenience, their detailed parameters are also summarized in Table 2. As shown in Fig. S59,† upon excitation at 400 nm, the Al_4 precursor raw material displays an emission band at 400–700 nm and the highest emission peak at 487 nm, which may belong to the π → π* transition of organic ligands. Under the same excitation conditions, these cluster-assembled compounds **AlOC-168** to **AlOC-170** and **AlOC-173** to **AlOC-176** show similar emission peaks, which can be observed at 500, 520, 489, 533, 477, 505 and 510 nm, respectively. However, **AlOC-171** and **AlOC-172** have no obvious photoluminescence under ultraviolet light (360 nm). Compound **AlOC-174** exhibits a blue-shift (*ca.* 10 nm) in comparison with the Al_4 cluster, and it shows blue light. However, **AlOC-173** and **AlOC-176** display distinct red-shifts of *ca.* 20–50 nm, and their luminescent colours are viridescent and yellow, respectively (Fig. S60†). In these case, the ligand-based luminescence is dominant and the blue-shifted or red-shifted phenomenon may be attributed to metal–ligand/cluster coordinative interactions. Additionally, the rigidity of

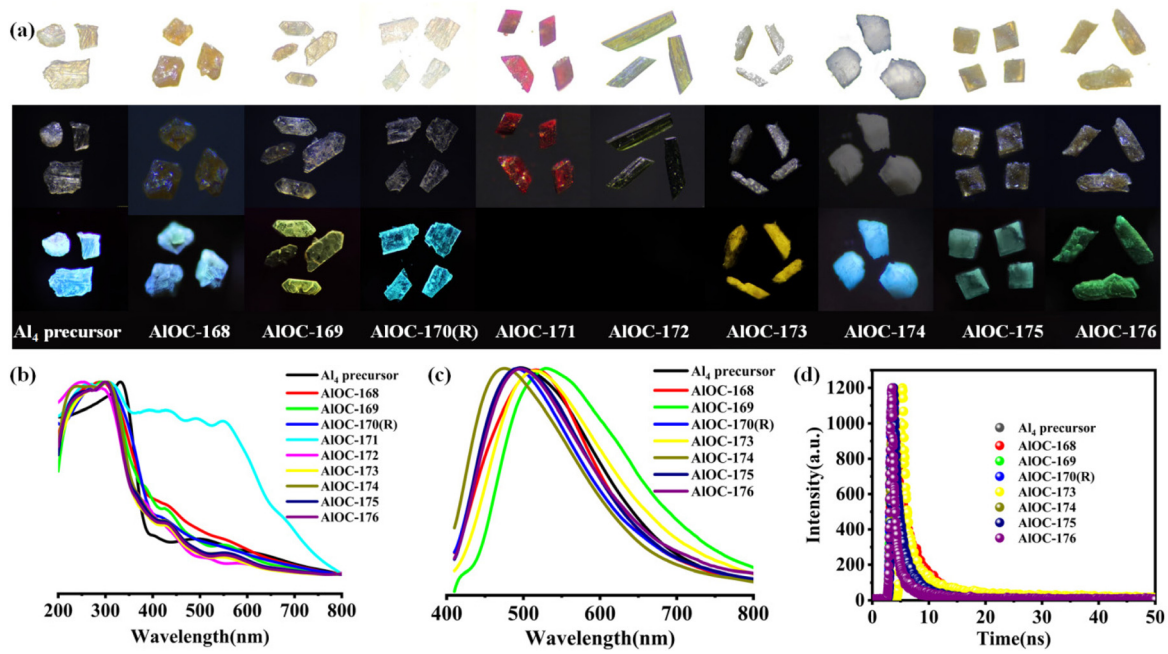

Fig. 3 The fluorescence properties of the pristine Al_4 precursor and the compounds from supracluster assembly. (a) Pictures of Al_4 precursor to **AlOC-176** crystals. The three images in each column from top to bottom show crystals in natural light, crystals in the dark without fluorescence irradiation, and crystals in the dark with fluorescence irradiation. (b) The UV/vis wavelengths of the Al_4 precursor to **AlOC-176**. (c) The emission wavelengths of the Al_4 precursor to **AlOC-176** except for those of **AlOC-171** and **AlOC-172**. (d) The transient fluorescence lifetime curves of the Al_4 precursor to **AlOC-176** except for those of **AlOC-171** and **AlOC-172**.

Table 2 The crucial photophysical parameters of the Al_4 precursor and compounds from supracluster assembly

Compound	UV/vis wavelength (nm)	Excitation wavelength (nm)	Emission wavelength (nm)	Fluorescence lifetime (ns)	β (cm GW^{-1})
Al_4 precursor	332	395	495	2.45	98
AlOC-168	288	395	515	3.24	200
AlOC-169	292	395	525	4.33	120
AlOC-170(*R*)	302	395	490	4.01	220
AlOC-171	306	395	455	0	130
AlOC-172	254	395	455	0	700
AlOC-173	301	395	515	4.25	750
AlOC-174	306	395	475	2.07	730
AlOC-175	300	395	495	2.02	710
AlOC-176	299	395	500	2.07	700

the ligands in the structure may also account for the fluorescence differences. The rigidity of the ligands in **AlOC-173** and **AlOC-169** is greater compared to that in other structures, and hence their fluorescence lifetimes are somewhat superior. In a word, the luminescent colour changes can be realized by different supracluster assembly behaviours.

Studies of third-order nonlinear optical (NLO) properties

Third-order nonlinear optical (NLO) materials are of particular importance for various applications including the optical limiting effect. It is reported that effects of larger conjugated systems and heavy metals have been proven to have positive influences on third-order nonlinear optical and optical limiting behavior.[49,52–54] Considering the presence of heavy metals and large conjugated chromophores, we then decided to study their third-order NLO properties. In order to ensure the stability of compounds **AlOC-168** to **AlOC-176**, the crystals of these materials are effectively dispersed into polydimethylsiloxanes (PDMSs) and then made into a thin film (named **AlOCs@PDMS** film), respectively. (The Experimental section provides detailed experimental information.) For better comparison, we also tested the third-order NLO properties of the starting Al_4 precursor by the same film-making method (Al_4 precursor@PDMS). The third-order NLO properties of these films were studied using a typical open-aperture *Z*-scan system with a nanosecond laser at 532 nm.

Precise control of the intramolecular coordination bonds and intermolecular non-covalent forces of clusters tunes charge transfer and band gap enhancement and ultimately improves the third-order nonlinear optical performance. Under an input laser pulse energy of 80 μJ, Al_4 precursor@PDMS to **AlOCs@PDMS** display obvious reverse-saturated absorption (RSA) behaviors and exhibit a sequentially enhanced optical limiting response from **AlOC-168** to **AlOC-176** (Fig. 4a and Table S4†). In order to quantitatively evaluate the NLO performance of the sample, the nonlinear absorption coefficient (β) (eqn (1)) of the sample was obtained from the best-fit curve:

$$T(z, s=1) = \frac{1}{\sqrt{\pi} q_0(z,0)} \int_{-\infty}^{\infty} \ln[1 + q_0(z,0) e^{-r^2}] dr \qquad (1)$$

Here, $q_0(z,0) = \beta I_0 L_{\text{eff}}$, where I_0 is the on-axis peak intensity at the focus ($z = 0$), $L_{\text{eff}} = [1-\exp(-\alpha l)]/\alpha$ denotes the effective thickness of the sample, α is the linear absorption coefficient, and l indicates the sample thickness. The values of β for Al_4 precursor@PDMS and **AlOCs@PDMS** composite films are 98, 200, 120, 220, 130, 700, 750, 730, 710, and 700 cm GW^{-1}, respectively (Fig. 4d). Compared with the Al_4 precursor, the introduced large conjugated ligands facilitate charge transfer between anion and cation groups, thus improving the third-order NLO performance. In the non-covalently assembled compounds (**AlOC-168** to **AlOC-172**), **AlOC-172** has relatively good nonlinear absorption due to its low bandgap and heavy metal effect. As for supracluster assembly *via* coordination bonds, compounds **AlOC-173** to **AlOC-176** exhibit better optical limiting responses, which is attributed to the coordination inter-

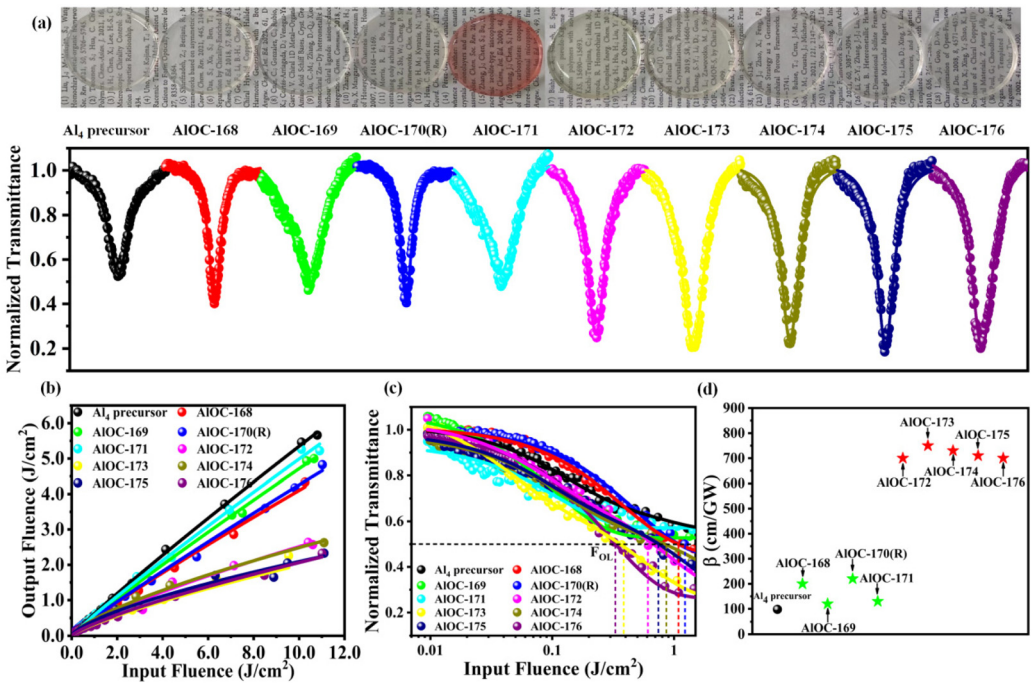

Fig. 4 The third-order NLO of the pristine Al_4 precursor and compounds from supracluster assembly. (a) The opening *Z*-scan curve at 532 nm of the samples. At the top of the *Z*-scan curves are photographs of the Al_4 precursor@PDMS and **AlOCs@PDMS** before (upper panel) and after (lower panel) applying 360 nm UV light. (b) Curves of output fluence *versus* input fluence for the Al_4 precursor, and **AlOC-168** to **AlOC-176**. (c) Plots of normalized transmittance *versus* input fluence for the Al_4 precursor, and **AlOC-168** to **AlOC-176**. (d) Comparison of the nonlinear absorption coefficients at a laser intensity of 80 μJ for Al_4 precursor@PDMS and **AlOCs@PDMS**.

action significantly enhancing charge transfer between anion and cation groups, thus improving the third-order NLO performance. The supercluster assembly strategy may serve as a reference for future performance enhancement. It is a direction worth exploring further. It is comparable to that of rare-earth metal or transition metal cluster-based materials,[55,56] although they are not comparable with metal-porphyrinic frameworks or porphyrin covalent organic frameworks (Table S5†).[57,58]

The curves of output fluence *versus* input fluence of such samples show that the output fluence linearly increases at low-incident fluence. At high-incident fluence, the output fluence deviates from linearity and shows a typical OL response (Fig. 4b). Their optical limiting threshold values (F_{OL}, defined as the input fluence at 50% linear transmittance) are 5.12 J cm^{-2} ($F_{OL\ Al4\ precursor}$), 1.09 J cm^{-2} ($F_{OL\ AlOC\text{-}168}$), 3.45 J cm^{-2} ($F_{OL\ AlOC\text{-}169}$), 1.23 J cm^{-2} ($F_{OL\ AlOC\text{-}170(R)}$), 3.59 J cm^{-2} ($F_{OL\ AlOC\text{-}171}$), 0.61 J cm^{-2} ($F_{OL\ AlOC\text{-}172}$), 0.39 J cm^{-2} ($F_{OL\ AlOC\text{-}173}$), 0.86 J cm^{-2} ($F_{OL\ AlOC\text{-}174}$), 0.75 J cm^{-2} ($F_{OL\ AlOC\text{-}175}$), and 0.33 J cm^{-2} ($F_{OL\ AlOC\text{-}176}$), respectively (Fig. 4c). In addition, we have carried out cycling experiments to verify the laser stability of **AlOCs@PDMS** materials. The results show that the RSA profiles of all third-order NLO materials have the same reproducibility after 4 or 8 cycles (Fig. S63–S72†).

Conclusions

In summary, by employing the Al_4 cluster as a precursor, a supracluster assembly strategy (including both non-covalent interaction and coordination bonds) was applied to construct a series of interesting cluster-based architectures. By introducing large π-conjugated phenanthroline- or phenylphosphine-type organic ligands, these cluster-assembled compounds showed different photoluminescent colors. The results showed that supracluster assembly *via* coordination bonds facilitates charge transfer and can effectively enhance the third-order NLO properties of cluster-based materials compared with those based on non-covalent bonds. This work not only demonstrates a general synthesis strategy based on a pre-designed precursor but also provides important guidance for stepwise tuning and optimization toward specific properties.

Experimental section

Synthesis of the Al_4 precursor

The synthesis of $(Me_2NH_2)_4[Al_4(L)_4(Cat)_2]$ (**AlOC-13**) is based on our previous work.[41] A mixture of $Al(O^iPr)_3$ (0.2 g, 0.98 mmol), 2,3-dihydroxybenzoic acid (H_3L, 0.4 g, 2.60 mmol), pyrazole (2 g, 29.38 mmol), and DMF (5 mL) was sealed in a 25 mL Teflon reactor and transferred to a preheated oven at 160 °C for 3 days. When cooled to room temperature, light brown crystals of **AlOC-13** were obtained (yield: 75% based on $Al(O^iPr)_3$). Amplification synthesis is also possible: using a 25 mL Teflon reactor, 0.27 g of **AlOC-13** can be obtained, and using a 50 mL Teflon reactor, 0.68 g of **AlOC-13** can be obtained.

Supracluster assembly based on the Al_4 precursor

By investigating the supracluster assembly behavior of the Al_4 cluster with metal ions (such as Ag Fe^{2+} and Cu^{2+}) in the presence of chelated ligands (like N,N-chelated (phenanthroline-type) or P,P-chelated (phenylphosphine-type) ligands) with diverse binding distances and angles, we successfully obtained a variety of cluster-based solids. A typical solvothermal synthesis of **AlOC-168** $(Me_2NH_2)_3[Ag(1,3\text{-}bdpp)_2][Al_4(L)_4(Cat)_2]\cdot$guests is described as follows: the Al_4 precursor (55 mg, 0.05 mmol) was dissolved in 2 mL of H_2O at 100 °C for 6 h. A mixture of 2 mL of precursor, silver perchlorate ($AgClO_4$, 14 mg, 0.07 mmol), 1,3-bis(diphenylphosphino)propane (1,3-bdpp, 45 mg, 0.11 mmol), EtOH (2 mL), and DMF (2 mL) was sealed in a 20 mL vial at 80 °C for 24 h. When cooled to room temperature, light brown crystals were obtained (yield: 75% based on the Al_4 precursor). The crystals were rinsed with EtOH and preserved in a sealed and dry environment. The synthetic procedure for other compounds is similar to that of **AlOC-168** but with different ligands and solvents. For the detailed synthesis, please refer to the ESI.†

Fabrication of Al_4 precursor@PDMS and AlOCs@PDMS

Al_4 precursor@PDMS and **AlOCs@PDMS** were prepared using Sylgard 184 (Dow Corning) by thoroughly mixing 10 parts base with 1 part curing agent. The coordinate crystals were mixed with the PDMS solution to form coordinate-dispersed PDMS suspension, and then the mixture suspension was added to a template and the template was placed in a vacuum oven at 60 °C for 6 hours. Finally, transparent and flexible Al_4 precursor@PDMS and **AlOCs@PDMS** were obtained.

Z-Scan measurements

The third-order NLO properties of the sample were evaluated by using the *Z*-scan technique. The excitation light source was an Nd:YAG laser with a repetition rate of 5 Hz. The laser pulse (period, 5 ns; wavelength, 532 nm) was split into two beams with a mirror. The pulse energies at the front and back of the samples were monitored using energy detectors 1 and 2. All of the measurements were conducted at room temperature. The sample was mounted on a computer-controlled translation stage that shifted each sample along the *z*-axis.

Author contributions

All authors contributed extensively to the work presented in this paper. J. Zhang and W.-H. Fang conceived the research project. F. Yang and R.-Y. Chen performed the synthesis, and characterization and optical property studies. T.-S. Wang and Y.-P. He helped with the crystallographic data refinement. W.-H. Fang and Y.-P. He wrote the manuscript and ESI† with input from the other authors.

Data availability

X-ray crystallographic data have been deposited at the Cambridge Crystallographic Data Centre (**https://www.ccdc.cam.ac.uk/**) with CCDC reference numbers 2303391 to 2303400† (single-crystal **AlOC-168** to **AlOC-176**).

Conflicts of interest

There are no conflicts to declare.

Acknowledgements

The research reported in this publication was supported by the National Natural Science Foundation of China (U23A20950, 22371278, and 92261108), the Science Fund for Distinguished Young Scholars of Fujian Province (2021J06035), the Funding of the Fujian Provincial Chemistry Discipline Alliance (50025401), and the Youth Innovation Promotion Association of the Chinese Academy of Sciences (Y2021081).

References

1 J. L. Segura, S. Royuela and M. Mar Ramos, Post-synthetic modification of covalent organic frameworks, *Chem. Soc. Rev.*, 2019, **48**, 3903–3945.
2 H. Wang, Y. Jin, N. Sun, W. Zhang and J. Jiang, Well-Defined, Versatile and Recyclable Half-Sandwich Nickelacarborane Catalyst for Selective Carbene-Transfer Reactions, *Chem. Soc. Rev.*, 2021, **50**, 8874–8886.
3 S. Mandal, S. Natarajan, P. Mani and A. Pankajakshan, Post-Synthetic Modification of Metal-Organic Frameworks Toward Applications, *Adv. Funct. Mater.*, 2021, **31**, 2006291.
4 T. Chen and D. Zhao, Post-synthetic modification of metal-organic framework-based membranes for enhanced molecular separations, *Coord. Chem. Rev.*, 2023, **491**, 215259.
5 H. Ding, A. Mal and C. Wang, Tailored covalent organic frameworks by post-synthetic modification, *Mater. Chem. Front.*, 2020, **4**, 113–127.
6 J. Liu, Z. Wang, P. Cheng, M. J. Zaworotko, Y. Chen and Z. Zhang, Post-synthetic modifications of metal-organic cages, *Nat. Rev. Chem.*, 2022, **6**, 339–356.
7 P. Waeles, M. Gauthier and F. Coutrot, Challenges and Opportunities in the Post-Synthetic Modification of Interlocked Molecules, *Angew. Chem., Int. Ed.*, 2021, **60**, 16778–16799.
8 F. A. El-malek and A. Steinbuchel, Post-synthetic Enzymatic and Chemical Modifications for Novel Sustainable Polyesters, *Front. Bioeng. Biotechnol.*, 2022, **9**, 817023.
9 E. M. El-Sayed, Y.-D. Yuan, D. Zhao and D. Yuan, Zirconium Metal-Organic Cages: Synthesis and Applications, *Acc. Chem. Res.*, 2022, **55**, 1546–1560.
10 Y.-P. He, L.-B. Yuan, J.-S. Song, G.-H. Chen, Q. Lin, C. Li, L. Zhang and J. Zhang, Optical Resolution of the Water-Soluble Ti_4(embonate)$_6$ Cages for Enantioselective Recognition of Chiral Drugs, *Chem. Mater.*, 2018, **30**, 7769–7775.
11 G.-H. Chen, H.-Z. Li, Y.-P. He, S.-H. Zhang, X. Yi, F.-P. Liang, L. Zhang and J. Zhang, Ti4(embonate)6 Based Cage-Cluster Construction in a Stable Metal–Organic Framework for Gas Sorption and Separation, *Cryst. Growth Des.*, 2019, **20**, 29–32.
12 Y.-P. He, L.-B. Yuan, G.-H. Chen, Q.-P. Lin, F. Wang, L. Zhang and J. Zhang, Water-Soluble and Ultrastable Ti_4L_6 Tetrahedron with Coordination Assembly Function, *J. Am. Chem. Soc.*, 2017, **139**, 16845–16851.
13 R.-Y. Chen, G.-H. Chen, Y.-P. He and J. Zhang, Coordination Assembly of Tetrahedral Ti_4(embonate)$_6$ Cages with Alkaline-Earth Metal Ions, *Chin. J. Struct. Chem.*, 2022, **41**, 2201001–2201006.
14 G.-H. Chen, Y.-P. He, Y. Yu, H. Lv, S. Li, F. Wang, Z.-G. Gu and J. Zhang, Post-Assembly Modification of Homochiral Titanium-Organic Cages for Recognition and Separation of Molecular Isomers, *Angew. Chem., Int. Ed.*, 2023, **62**, e202300726.
15 A. J. Gosselin, A. M. Antonio, K. J. Korman, M. M. Deegan, G. P. A. Yap and E. D. Bloch, Elaboration of Porous Salts, *J. Am. Chem. Soc.*, 2021, **143**, 14956–14961.
16 E. J. Gosselin, G. E. Decker, A. M. Antonio, G. R. Lorzing, G. P. A. Yap and E. D. Bloch, A Charged Coordination Cage-Based Porous Salt, *J. Am. Chem. Soc.*, 2020, **142**, 9594–9598.
17 G. Liu, Y. Di Yuan, J. Wang, Y. Cheng, S. B. Peh, Y. Wang, Y. Qian, J. Dong, D. Yuan and D. Zhao, Process-Tracing Study on the Postassembly Modification of Highly Stable Zirconium Metal-Organic Cages, *J. Am. Chem. Soc.*, 2018, **140**, 6231–6234.
18 G. Liu, X. Zhang, Y. Di Yuan, H. Yuan, N. Li, Y. Ying, S. B. Peh, Y. Wang, Y. Cheng, Y. Cai, Z. Gu, H. Cai and D. Zhao, Thin-Film Nanocomposite Membranes Containing Water-Stable Zirconium Metal–Organic Cages for Desalination, *ACS Mater. Lett.*, 2021, **3**, 268–274.
19 J. Liu, W. Duan, J. Song, X. Guo, Z. Wang, X. Shi, J. Liang, J. Wang, P. Cheng, Y. Chen, M. J. Zaworotko and Z. Zhang, Self-Healing Hyper-Cross-Linked Metal-Organic Polyhedra (HCMOPs) Membranes with Antimicrobial Activity and Highly Selective Separation Properties, *J. Am. Chem. Soc.*, 2019, **141**, 12064–12070.
20 D. Nam, J. Huh, J. Lee, J. H. Kwak, H. Y. Jeong, K. Choi and W. Choe, Cross-linking Zr-based metal-organic polyhedra via postsynthetic polymerization, *Chem. Sci.*, 2017, **8**, 7765–7771.
21 B. S. Pilgrim, D. A. Roberts, T. G. Lohr, T. K. Ronson and J. R. Nitschke, Signal transduction in a covalent post-assembly modification cascade, *Nat. Chem.*, 2017, **9**, 1276–1281.
22 D. A. Roberts, B. S. Pilgrim, J. D. Cooper, T. K. Ronson, S. Zarra and J. R. Nitschke, Post-assembly Modification of Tetrazine-Edged $Fe(II)_4L_6$ Tetrahedra, *J. Am. Chem. Soc.*, 2015, **137**, 10068–10071.

23 T. K. Ronson, B. S. Pilgrim and J. R. Nitschke, Pathway-Dependent Post-assembly Modification of an Anthracene-Edged $M(II)_4L_6$ Tetrahedron, *J. Am. Chem. Soc.*, 2016, **138**, 10417–10420.
24 Q.-Q. Yan, L.-P. Zhou, H.-Y. Zhou, Z. Wang, L.-X. Cai, X.-Q. Guo, X. Q and Q.-F. Sun, Metallopolymers cross-linked with self-assembled Ln(4)L(4) cages, *Dalton Trans.*, 2019, **48**, 7080–7084.
25 L.-L. Yan, C.-H. Tan, G.-L. Zhang, L.-P. Zhou, J.-C. Bunzli and Q.-F. Sun, Stereocontrolled Self-Assembly and Self-Sorting of Luminescent Europium Tetrahedral Cages, *J. Am. Chem. Soc.*, 2015, **137**, 8550–8555.
26 G. R. Lorzing, A. J. Gosselin, B. A. Trump, A. H. P. York, A. Sturluson, C. A. Rowland, G. P. A. Yap, C. M. Brown, C. M. Simon and E. D. Bloch, Understanding Gas Storage in Cuboctahedral Porous Coordination Cages, *J. Am. Chem. Soc.*, 2019, **141**, 12128–12138.
27 G. R. Lorzing, B. A. Trump, C. M. Brown and E. D. Bloch, Selective Gas Adsorption in Highly Porous Chromium(II)-Based Metal–Organic Polyhedra, *Chem. Mater.*, 2017, **29**, 8583–8587.
28 J. Park, Z. Perry, Y. P. Chen, J. Bae and H. C. Zhou, Chromium(II) Metal-Organic Polyhedra as Highly Porous Materials, *ACS Appl. Mater. Interfaces*, 2017, **9**, 28064–28068.
29 T. Zhang, J. Brown, R. J. Oakley and C. F. J. Faul, Towards functional nanostructures: Ionic self-assembly of polyoxometalates and surfactants, *Curr. Opin. Colloid Interface Sci.*, 2009, **14**, 62–70.
30 H. N. Miras, J. Yan, D.-L. Long and L. Cronin, Engineering polyoxometalates with emergent properties, *Chem. Soc. Rev.*, 2012, **41**, 7403–7430.
31 M.-P. Santoni, G. S. Hanan and B. Hasenknopf, Covalent multi-component systems of polyoxometalates and metal complexes: Toward multi-functional organic–inorganic hybrids in molecular and material sciences, *Coord. Chem. Rev.*, 2014, **281**, 64–85.
32 V. Das, R. Kaushik and F. Hussain, Heterometallic 3d-4f polyoxometalates: An emerging field with structural diversity to multiple applications, *Coord. Chem. Rev.*, 2020, **413**, 213271.
33 J. M. Cameron, G. Guillemot, T. Galambos, S. S. Amin, E. Hampson, K. Mall Haidaraly, G. N. Newton and G. Izzet, Supramolecular assemblies of organo-functionalised hybrid polyoxometalates: from functional building blocks to hierarchical nanomaterials, *Chem. Soc. Rev.*, 2022, **51**, 293–328.
34 N. Ogiwara, T. Iwano, T. Ito and S. Uchida, Proton conduction in ionic crystals based on polyoxometalates, *Coord. Chem. Rev.*, 2022, **462**, 214524.
35 H. Choi, Y. U. Kwon and O. H. Han, Nanocomposite gels between $(V_{10}O_{28})^{-6}$ and $[AlO_4(Al_{12}(OH)_{24}(H_2O)_{12})]^{7+}$ polyoxometalate clusters, *Chem. Mater.*, 1999, **11**, 1641–1643.
36 Y.-J. Liu, H.-F. Su, Y.-F. Sun, S.-T. Wang, C.-Y. Zhang, W.-H. Fang and J. Zhang, Supracluster Assembly of Archimedean Cages with 72 Hydrogen Bonds for the Aldol Addition Reaction, *Angew. Chem., Int. Ed.*, 2023, **62**, e202309971.
37 D. Xia, P. Wang, X. Ji, N. M. Khashab, J. L. Sessler and F. Huang, Functional Supramolecular Polymeric Networks: The Marriage of Covalent Polymers and Macrocycle-Based Host-Guest Interactions, *Chem. Rev.*, 2020, **120**, 6070–6123.
38 Y. Xia, T. D. Nguyen, M. Yang, B. Lee, A. Santos, P. Podsiadlo, Z. Tang, S. C. Glotzer and N. A. Kotov, Self-assembly of self-limiting monodisperse supraparticles from polydisperse nanoparticles, *Nat. Nanotechnol.*, 2011, **6**, 580–587.
39 B. K. Teo, H. Zhang and X. Shi, The First Example of a Trimetallic Biicosahedral Supracluster and Its Implication for the Vertex-Sharing Polyicosahedral Growth, *J. Am. Chem. Soc.*, 1993, **115**, 8489–8490.
40 M. J. Dale, P. J. Dyson, B. F. G. Johnson, P. R. R. LangridgeSmith and H. T. Yates, Laser-desorption mass spectrometry of $[Ru_6C(CO)_{17}]$ and its derivatives: Cluster aggregation in the gas phase, *J. Chem. Soc. Dalton*, 1996, 771–774.
41 L. Geng, C.-H. Liu, S.-T. Wang, W.-H. Fang and J. Zhang, Designable Aluminum Molecular Rings: Ring Expansion and Ligand Functionalization, *Angew. Chem., Int. Ed.*, 2020, **59**, 16735–16740.
42 S.-T. Wang, S.-H. Zhang, W.-H. Fang and J. Zhang, Stepwise Coordination Assembly Approach toward Aluminum-Lanthanide-based Compounds, *Inorg. Chem.*, 2020, **59**, 13760–13766.
43 S. Yao, W.-H. Fang, Y. Sun, S.-T. Wang and J. Zhang, Mesoporous Assembly of Aluminum Molecular Rings for Iodine Capture, *J. Am. Chem. Soc.*, 2021, **143**, 2325–2330.
44 Y.-J. Liu, Y.-F. Sun, S.-H. Shen, S.-T. Wang, Z.-H. Liu, W.-H. Fang, D. S. Wright and J. Zhang, Water-stable porous Al24 Archimedean solids for removal of trace iodine, *Nat. Commun.*, 2022, **13**, 6632.
45 Z.-H. Liu, S.-H. Shen, C.-Y. Zhang, J. Niu, Q.-H. Li, J. Zhang and W.-H. Fang, Design and synthesis of a deep-cavity aluminium-organic macrocycle to trap dyes and generate enhanced non-linear optical performance, *Inorg. Chem. Front.*, 2024, **11**, 3777–3785.
46 S.-T. Wang, X. Qi, R.-Q. Chen, W.-H. Fang and J. Zhang, Two solvent-dependent Al_{16} nanorings: design, synthesis and nonlinear optical limiting behavior, *Inorg. Chem. Front.*, 2024, **11**, 462–469.
47 Y. Zhang, Q.-H. Li, W.-H. Fang and J. Zhang, Aluminum molecular rings bearing amino-polyalcohol for iodine capture, *Inorg. Chem. Front.*, 2022, **9**, 592–598.
48 D. Dini, M. J. Calvete and M. Hanack, Nonlinear Optical Materials for the Smart Filtering of Optical Radiation, *Chem. Rev.*, 2016, **116**, 13043–13233.
49 W.-H. Zhang, Q. Liu and J.-P. Lang, Heterometallic transition metal clusters and cluster-supported coordination polymers derived from Tp- and Tp*-based Mo(W) sulfido precursors, *Coord. Chem. Rev.*, 2015, **293**, 187–210.
50 K. Nakashima, R. Suizu, S. Morishita, N. Tsurumachi, M. Funahashi, H. Masu, R. Ozawa, K. Nakamura and K. Awaga, Enhanced Circularly Polarized Luminescence by

a Homochiral Guest–Host Interaction in Gyroidal MOFs, $[Ru(bpy)_3]$ $[M_2(ox)_3]$ (bpy = 2,2′-Bipyridyl, ox = Oxalate, M = Zn, Mn), *ACS Mater. Au*, 2023, **3**, 201–205.

51 M. Saqlain, H. M. Zohaib, S. Qamar, H. Malik and H. Li, Strategies for the enhancement of CPL properties, *Coord. Chem. Rev.*, 2024, **501**, 215559.

52 S.-J. Bao, Z.-M. Xu, Y. Ju, Y.-L. Song, H. Wang, Z. Niu, X. Li, P. Braunstein and J.-P. Lang, The Covalent and Coordination Co-Driven Assembly of Supramolecular Octahedral Cages with Controllable Degree of Distortion, *J. Am. Chem. Soc.*, 2020, **142**, 13356–13361.

53 Z.-K. Wang, M.-H. Du, P. Braunstein and J.-P. Lang, A Cut-to-Link Strategy for Cubane-Based Heterometallic Sulfide Clusters with Giant Third-Order Nonlinear Optical Response, *J. Am. Chem. Soc.*, 2023, **145**, 9982–9987.

54 Q. Liu, W.-H. Zhang and J.-P. Lang, Versatile thiomolybdate (thiotungstate)-copper-sulfide clusters and multidimensional polymers linked by cyanides, *Coord. Chem. Rev.*, 2017, **350**, 248–274.

55 H. Hou, Y. Wei, Y. Song, Y. Fan and Y. Zhu, First octameric ellipsoid lanthanide (III) complexes: crystal structure and nonlinear optical absorptive and refractive properties, *Inorg. Chem.*, 2004, **43**, 1323–1327.

56 P. Mathur, S. Ghose, M. M. Hossain, C. Satyanarayana, S. Banerjee, G. R. Kumar, P. B. Hitchcock and J. F. Nixon, Phosphaalkyne-bridged clusters: synthesis, characterization, and nonlinear optical properties of Fe_4Se_2(μ-Se_2PCBut)$(CO)_{11}$, *Organometallics*, 1997, **16**, 3815–3818.

57 D.-J. Li, Q.-H. Li, Z.-R. Wang, Z.-Z. Ma, Z.-G. Gu and J. Zhang, Interpenetrated Metal-Porphyrinic Framework for Enhanced Nonlinear Optical Limiting, *J. Am. Chem. Soc.*, 2021, **143**, 17162–17169.

58 B. P. Biswal, S. Valligatla, M. Wang, T. Banerjee, N. A. Saad, B. M. K. Mariserla, N. Chandrasekhar, D. Becker, M. Addicoat, I. Senkovska, R. Berger, D. N. Rao, S. Kaskel and X. Feng, Nonlinear Optical Switching in Regioregular Porphyrin Covalent Organic Frameworks, *Angew. Chem., Int. Ed.*, 2019, **58**, 6896–6900.